J|A|C|S
ARTICLES
Published on Web 02/20/2002

Molecular Structures and Excited States of $CpM(CO)_2$ (Cp = η^5-C_5H_5; M = Rh, Ir) and $[Cl_2Rh(CO)_2]^-$. Theoretical Evidence for a Competitive Charge Transfer Mechanism

Zhenming Hu,[†] Russell J. Boyd,*[,†] and Hiroshi Nakatsuji[‡]

Contribution from the Department of Chemistry, Dalhousie University, Halifax, Nova Scotia, Canada B3H 4J3, and Department of Synthetic Chemistry and Biological Chemistry, Graduate School of Engineering, Kyoto University, Sakyo-ku, Kyoto 606-8501, Japan

Received March 28, 2001. Revised Manuscript Received November 12, 2001

Abstract: Molecular structures and excited states of $CpM(CO)_2$ (Cp = η^5-C_5H_5; M = Rh, Ir) and $[Cl_2Rh(CO)_2]^-$ complexes have been investigated using the B3LYP and the symmetry-adapted cluster (SAC)/SAC−configuration interaction (SAC−CI) theoretical methods. All the dicarbonyl complexes have singlet ground electronic states with large singlet−triplet separations. Thermal dissociations of CO from the parent dicarbonyls are energetically unfavorable. CO thermal dissociation is an activation process for $[Cl_2Rh(CO)_2]^-$ while it is a repulsive potential for $CpM(CO)_2$. The natures of the main excited states of $CpM(CO)_2$ and $[Cl_2Rh(CO)_2]^-$ are found to be quite different. For $[Cl_2Rh(CO)_2]^-$, all the strong transitions are identified to be metal to ligand CO charge transfer (MLCT) excitations. A significant feature of the excited states of $CpM(CO)_2$ is that both MLCT excitation and a ligand Cp to metal and CO charge transfer excitation are strongly mixed in the higher energy states with the latter having the largest oscillator strength. A competitive charge transfer excited state has therefore been identified theoretically for $CpRh(CO)_2$ and $CpIr(CO)_2$. The wavelength dependence of the quantum efficiencies for the photoreactions of $CpM(CO)_2$ reported by Lees et al. can be explained by the existence of two different types of excited states. The origin of the low quantum efficiencies for the C−H/Si−H bond activations of $CpM(CO)_2$ can be attributed to the smaller proportion of the MLCT excitation in the higher energy states.

I. Introduction

Since the discovery that the d^8 transition-metal dicarbonyls such as $CpM(CO)_2$ and $Cp^*M(CO)_2$ (Cp = η^5-C_5H_5, Cp* = η^5-$C_5(CH_3)_5$, M = Rh, Ir) have the unique ability to activate the normally unreactive C−H bonds of alkanes upon light excitation,[1,2] numerous experimental efforts have been made to understand their structures, spectra, and the details of the photoreaction mechansims. Although considerable progress has been made over the past decade, the identity of the primitive photoproducts and their reactivities toward C−H/Si−H bond activations and ligand substitution are still actively debated. Various experiments including low-temperature matrix isolation,[3] laser-flash photolysis,[4] kinetic and spectroscopic studies in the gas phase,[5] and in liquid noble gases[6] suggest a dissociative mechanism in which the first step of the reaction is the photoinitiated loss of CO, forming a coordinatively unsaturated intermediate of (η^5-C_5R_5)M(CO) (R = H, CH_3).

On the other hand, Lees et al.[7,8] have performed a number of photochemical quantum efficiency experiments for the ligand photosubstitution and C−H/Si−H bond activation reactions of $CpIr(CO)_2$, $CpRh(CO)_2$, $Cp^*Rh(CO)_2$, and $(HBPz_3^*)Rh(CO)_2$ (HBPz* = 3,5-dimethylpyrazolyl). An important observation in their studies[7,8] is that the quantum efficiencies are dependent both on the excitation wavelength and on the ligand involved. The short-wavelength irradiation at 313 nm (3.96 eV) of $CpRh(CO)_2$ gives a quantum efficiency of $\phi_{cr} > 0.1$ for ligand substitution and C−H/Si−H bond activations, while the long-wavelength irradiation at 458 nm (2.71 eV) gives a quantum efficiency of $\phi_{cr} \approx 0.001$ for ligand substitution. The photochemistry of $Cp^*Rh(CO)_2$ is analogous to $CpRh(CO)_2$, but the quantum efficiency values are lower by more than an order of magnitude.[7c] The study of $(HBPz_3^*)Rh(CO)_2$ irradiation reported a considerably larger quantum yield of $\phi_{cr} \approx 0.3$.[8] On the basis

* To whom correspondence should be addressed. E-mail: boyd@is.dal.ca.
[†] Dalhousie University.
[‡] Kyoto University.

(1) (a) Janowicz, A. H.; Bergman, R. G. *J. Am. Chem. Soc.* **1982**, *104*, 352. (b) Janowicz, A. H.; Bergman, R. G. *J. Am. Chem. Soc.* **1983**, *105*, 3929.
(2) Hoyano, J. K.; Graham, W. A. G. *J. Am. Chem. Soc.* **1982**, *104*, 3723. (b) Hoyano, J. K.; McMaster, A. D.; Graham, W. A. G. *J. Am Chem. Soc.* **1983**, *105*, 7190.
(3) (a) Haddleton, D. M.; McCramley, A.; Perutz, R. N. *J. Am. Chem. Soc.* **1988**, *110*, 1810. (b) Rest, A. J.; Whitwell, I.; Graham, W. A. G.; Hoyano, J. K.; McMaster, A. D. *J. Chem. Soc., Dalton Trans.* **1987**, 1181.
(4) (a) Belt, S. T.; Grevels, F. W.; Koltzbücher, W. E.; McCamley, A.; Perutz, R. N. *J. Am. Chem. Soc.* **1989**, *111*, 8373. (b) Dougherty, T. P.; Grubbs, W. T.; Heiweil, E. J. *J. Phys. Chem.* **1994**, *98*, 9396.
(5) Wasserman, E. P.; Moore, C. B.; Bergman, R. G. *Science* **1992**, *255*, 315.
(6) (a) Weiller, B. H.; Wasserman, E. P.; Bergman, R. G.; Moore, C. B.; Pimentel, G. C. *J. Am Chem. Soc.* **1989**, *111*, 8288. (b) Weiller, B. H.; Wasserman, E. P.; Moore, C. B.; Bergman, R. G. *J. Am Chem. Soc.* **1993**, *115*, 4326.
(7) (a) Marx, D. E.; Lees, A. J. *Inorg. Chem.* **1988**, *27*, 1121. (b) Drolet, D. P.; Lees, A. J. *J. Am. Chem. Soc.* **1990**, *112*, 5878. (c) Drolet, D. P.; Lees, A. J. *J. Am. Chem. Soc.* **1992**, *114*, 4186. (d) Purwoko, A. A.; Lees, A. J. *J. Organomet. Chem.* **1995**, *504*, 107. (e) Dunwoody, N.; Lees, A. J. *Organometallics* **1997**, *16*, 5770.
(8) (a) Purwoko, A. A.; Lees, A. J. *Inorg. Chem.* **1995**, *34*, 424. (b) Lees, A. J. *J. Organomet. Chem.* **1998**, *554*, 1.

10.1021/ja0108178 CCC: $22.00

Scheme 1. Illustration of the Molecular Structures of (a) $CpRh(CO)_2$ (C_s), (b) $CpIr(CO)_2$ (C_s), and (c) $[Cl_2Rh(CO)_2]^-$ (C_{2v})

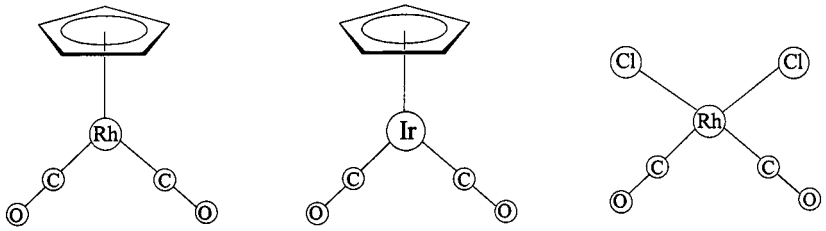

of their experimental results, Lees et al.[7c−e,8] concluded that two types of excited states with distinct reactivities are involved in the photochemistry of both $CpRh(CO)_2$ and $Cp^*Rh(CO)_2$, and consequently, two different reaction intermediates are implicated in the mechanism. The ligand photosubstitution takes place predominantly via an associative mechanism in which a ring slippage ($\eta^5-\eta^3$) is the preliminary step and the intermolecular C−H/Si−H bond activations proceed via the dissociative mechanism.[7]

Another important question that needs to be clarified is the origin of the low quantum efficiencies for the C−H bond activation of $Cp^*M(CO)_2$ and $CpM(CO)_2$. A recent ultrafast spectroscopic study of $Cp^*M(CO)_2$ (M = Rh, Ir)[9] suggested that there are lower lying excited states below the strong metal to ligand CO charge transfer (MLCT) band. Excitation into these states does not lead to CO dissociation. Instead, most of the molecules relax to the ground state in a short time. However, the exact natures of the excited states remain unknown.

There are several theoretical studies in the literature of the oxidative addition reaction between methane and transition-metal complexes.[10−14] All the theoretical studies have focused on the reaction energy profile of the C−H bond activation on the basis of the assumption that the coordinatively unsaturated monocarbonyl CpM(CO) is the key intermediate. Theoretical investigations of the excited states should be valuable for understanding the nature of the photochemistry of these dicarbonyl complexes.

There are three principal objectives in the present study. The first objective is to determine the molecular structures and electronic ground states of $CpM(CO)_2$ and $[Cl_2Rh(CO)_2]^-$ (Scheme 1). The potential energy surfaces of the thermal dissociations of CO from $CpM(CO)_2$ and $[Cl_2Rh(CO)_2]^-$ should also be discussed to understand the dissociation mechanism and to evaluate the energy requirement for the generation of the monocarbonyls under thermal conditions. The molecular and electronic structures of the monocarbonyls CpM(L) (L = CO, PH_3) have already been discussed by Ziegler et al.[11] and Hoffmann et al.,[15] and the thermal dissociation energies of CO from $CpM(CO)_2$ have also been evaluated by Ziegler et al.[11] The second objective is to study the excited states of the complexes shown in Scheme 1. To the best of our knowledge, no theoretical studies of the excited states of these molecules have been reported. It will be interesting to compare the similarities and differences of the excited states of these complexes, and more importantly, to understand the exact natures of the excited states. The third objective is to provide theoretical insight into the photochemistry of $CpM(CO)_2$ and $[Cl_2Rh(CO)_2]^-$ and to clarify the origin of the low quantum efficiencies for the C−H bond activation of $CpRh(CO)_2$ and $CpIr(CO)_2$.

II. Computational Methods

Molecular structures and the potential energy surfaces of CO thermal dissociations from the dicarbonyls were calculated using the B3LYP density functional method as implemented in the Gaussian 98[16] suite of programs. The details of the B3LYP method have been presented in the literature.[16−18] Geometry optimizations were carried out for the complexes in their singlet and lowest triplet states and also for all the species in the thermal dissociation processes. The standard 6-311G-(d,p)[19] basis set was used for carbon, oxygen, chlorine, and hydrogen. The Hay−Wadt[20] 17-valence electron relativistic effective core potentials were used for Rh and Ir atoms where the 4s and 4p electrons of Rh and the 5s and 5p electrons of Ir were treated explicitly as valence electrons. The valence electrons of Rh were described by the (5s6p4d/3s3p2d) basis set and those of Ir were described by the (5s6p3d/3s3p2d) basis set.[19] The method and the basis sets used have been confirmed to give reliable geometries and energetics of transition-metal carbonyl complexes in our previous paper.[21]

The excited singlet states of the three complexes were calculated using the symmetry-adapted cluster (SAC)/SAC−configuration interaction (SAC−CI) method with the local module.[22] The details of the SAC/SAC−CI for calculating ground and excited states of molecules have been presented elsewhere.[22−26] This method has been applied success-

(9) Bromberg, S. E.; Lian, T.; Bergman, R. G.; Harris, C. B. *J. Am. Chem. Soc*. **1996**, *118*, 2069.
(10) Saillard, J. Y.; Hoffmann, R. *J. Am. Chem. Soc*. **1984**, *106*, 2006.
(11) Ziegler, T.; Tschinke, V.; Fan, L.; Becke, A. D. *J. Am. Chem. Soc*. **1989**, *111*, 9177.
(12) Song, J.; Hall, M. B. *Organometallics* **1993**, *12*, 3118.
(13) Musaev, D. G.; Morokuma, K. *J. Am. Chem. Soc*. **1995**, *117*, 799.
(14) Siegbahn, P. E. M. *J. Am. Chem. Soc*. **1996**, *118*, 1487.
(15) Hoffmann, R.; Padmanabhan, M. *Organometallics* **1983**, *2*, 1273.
(16) Frisch, M. J.; Trucks, G. W.; Schlegel, H. B.; Scuseria, G. E.; Robb, M. A.; Cheeseman, J. R.; Zakrzewski, V. G.; Montgomery, J. A.; Stratmann, R. E.; Burant, J. C.; Dapprich, S.; Millam, J. M.; Daniels, A. D.; Kudin, K. N.; Strain, M. C.; Farkas, O.; Tomasi, J.; Barone, V.; Cossi, M.; Cammi, R.; Mennucci, B.; Pomelli, C.; Adamo, C.; Clifford, S.; Ochterski, J.; Petersson, G. A.; Ayala, P. Y.; Cui, Q.; Morokuma, K.; Malick, D. K.; Rabuck, A. D.; Raghavachari, K.; Foresman, J. B.; Cioslowski, J.; Ortiz, J. V.; Stefanov, B. B.; Liu, G.; Liashenko, A.; Piskorz, P.; Komaromi, I.; Gomperts, R.; Martin, R. L.; Fox, D. J.; Keith, T.; Al-Laham, M. A.; Peng, C. Y.; Nanayakkara, A.; Gonzalez, C.; Challacombe, M.; Gill, P. M. W.; Johnson, B.; Chen, W.; Wong, M. W.; Andres, J. L.; Gonzalez, C.; Head-Gordon, M.; Replogle, E. S.; Pople, J. A. *GAUSSIAN 98*, Revision A.5; Gaussian, Inc.: Pittsburgh, PA, 1998.
(17) Becke, A. D. *J. Chem. Phys*. **1993**, *98*, 5648.
(18) Stephens, P. J.; Devlin, F. J.; Chabalowski, C. F.; Frisch, M. J. *J. Phys. Chem*. **1994**, *98*, 11623.
(19) *EMSL Gaussian Basis Set Order Form.* Basis sets were obtained from the Extensible Computational Chemistry Environment Basis Set Database, Version, as developed and distributed by the Molecular Science Computing Facility, Environmental and Molecular Sciences Laboratory which is part of the Pacific Northwest Laboratory, P.O. Box 999, Richland, WA 99352, USA.
(20) Hay, P. J.; Wadt, W. R. *J. Chem. Phys*. **1985**, *82*, 270.
(21) Hu, Z. M.; Boyd, R. J. *J. Chem. Phys*. **2000**, *113*, 9393.
(22) Nakatsuji, H.; Hada, M.; Ehara, M.; Hasegawa, J.; Nakajima, T.; Nakai, H.; Kitao, O.; Toyota, K. SAC/SAC−CI program system (SAC−CI96) for calculating ground, excited, ionized, and electron attached states and singlet-to-septet spin multiplicities.
(23) Nakatsuji, H.; Hirao, K. *J. Chem. Phys*. **1978**, *68*, 2053.

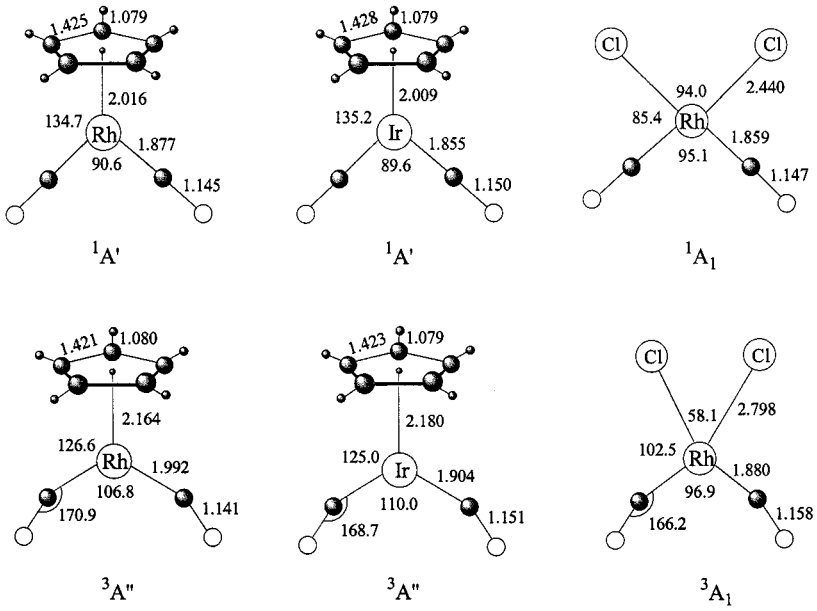

Figure 1. Optimized geometries of $CpRh(CO)_2$, $CpIr(CO)_2$, and $[Cl_2Rh(CO)_2]^-$ in their singlet $^1A'$ or $^1A_1$ and triplet $^3A''$ or $^3A_1$ states using the B3LYP method. The large shaded circles denote carbon atoms, the blank circles denote the oxygen atoms, and the small shaded circles denote the hydrogen atoms, respectively.

fully to the excitation spectra and to the reactions of several transition-metal complexes.[26−30] The basis sets used for the excited-state calculations are essentially the same as those described above except for hydrogen for which the standard 6-311G(d)[19] basis set was used instead. The total numbers of contracted basis functions are 199 for $CpM(CO)_2$ and 146 for $[Cl_2Rh(CO)_2]^-$. The number of occupied orbitals is 40 in each case.

In the present study, we have calculated eight singlet excited states for each molecule. In the SAC/SAC−CI calculations, six 1s core molecular orbitals of C, O, and Cl and six highest virtual orbitals were frozen for $[Cl_2Rh(CO)_2]^-$ and nine 1s core molecular orbitals of C and O and nine highest virtual orbitals were frozen for $CpM(CO)_2$, which result in active spaces of 31 occupied orbitals and 150 virtual orbitals for $CpM(CO)_2$ and 34 occupied orbitals and 100 virtual orbitals for $[Cl_2Rh(CO)_2]^-$, respectively. The energy thresholds for perturbation selection were 1.0×10^{-5} au for the ground state and 1.0×10^{-6} au for the excited states, respectively. The main reference configurations from SE−CI with a coefficient greater than 0.1 were included in the SAC−CI calculations.

III. Results and Discussions

A. Molecular Structures of $CpM(CO)_2$ and $[Cl_2Rh(CO)_2]^-$. As shown in Scheme 1, the two CO groups are equivalent in the C_s structures of $CpRh(CO)_2$ and $CpIr(CO)_2$ and the C_{2v} structure of $[Cl_2Rh(CO)_2]^-$. $[Cl_2Rh(CO)_2]^-$ has a square-planar structure, as already confirmed in our previous paper.[21] To determine the ground electronic state, the geometrical parameters of $CpRh(CO)_2$, $CpIr(CO)_2$, and $[Cl_2Rh(CO)_2]^-$ for both the singlet and the lowest triplet states were optimized. The optimized structures are shown in Figure 1. The electronic singlet and triplet states of $CpM(CO)_2$ are found to be $^1A'$ and $^3A''$ and those of $[Cl_2Rh(CO)_2]^-$ are $^1A_1$ and $^3A_1$, respectively.

Some geometrical changes from the singlet to the triplet states are apparent from Figure 1. The M−C−O bond is essentially linear in the singlet states while it is bent in the triplet states. For $CpRh(CO)_2$ and $CpIr(CO)_2$, the C−M−C bond angle is increased from about 90° in the singlet states to 107° and 110° in the triplet states, and the Cp−M distances are also increased from 2.0 Å in the singlet states to 2.16 and 2.18 Å in the triplet states. The geometrical differences between $CpRh(CO)_2$ and $CpIr(CO)_2$ are small although the latter has a shorter M−C bond length. For $[Cl_2Rh(CO)_2]^-$, the Rh−Cl bond length and the Cl−Rh−Cl bond angle are dramatically changed from the singlet state to the triplet state. The energies of the triplet states are calculated to be much higher than those of the singlet states. The energy differences are 33.4 kcal/mol for $CpRh(CO)_2$, 46.4 kcal/mol for $CpIr(CO)_2$, and 59.7 kcal/mol for $[Cl_2Rh(CO)_2]^-$, respectively. It is obvious that the ground electronic states of the molecules are the singlet states. The singlet−triplet separations of the dicarbonyl $CpM(CO)_2$ presented here are substantially larger than those of the corresponding monocarbonyl CpM(CO). The singlet−triplet separations of CpM(CO) have been reported to be 1.2−6.0 kcal/mol with the singlet states being slightly more stable.[11]

B. Thermal Dissociation of CO from $CpM(CO)_2$ and $[Cl_2Rh(CO)_2]^-$. Although the CO thermal dissociation is believed to be an energetically demanding process, the dissociation energies are unknown experimentally. Also, it is not clear whether the dissociation is an activation process or a simple repulsive potential. We tried to answer these questions by studying the potential energy surfaces of CO thermal dissociations from the dicarbonyl complexes.

Figure 2 shows the optimized geometries of the parent dicarbonyl molecules and the corresponding monocarbonyl molecules in their ground singlet states. The geometries of the parent molecules are the same as the singlet state geometries

(24) Nakatsuji, H. *Chem. Phys. Lett.* **1978**, *59*, 362.
(25) Nakatsuji, H. *Chem. Phys. Lett.* **1979**, *67*, 329.
(26) Nakatsuji, H. In *Computational Chemistry: Reviews of Current Trends*; Leszczynski, J., Ed.; World Scientific: Singapore, 1997; Vol. 2.
(27) Hada, M.; Imai, Y.; Hidaka, M.; Nakatsuji, H. *J. Chem. Phys.* **1995**, *103*, 6993.
(28) Morita, H.; Nakai, H.; Hanada, H.; Nakatsuji, H. *Mol. Phys.* **1997**, *92*, 523.
(29) Nakatsuji, H.; Ehara, M.; Palmer, M. H.; Guest, M. F. *J. Chem. Phys.* **1992**, *97*, 2561.
(30) Nakatsuji, H.; Ehara, M. *J. Chem. Phys.* **1994**, *101*, 7658.

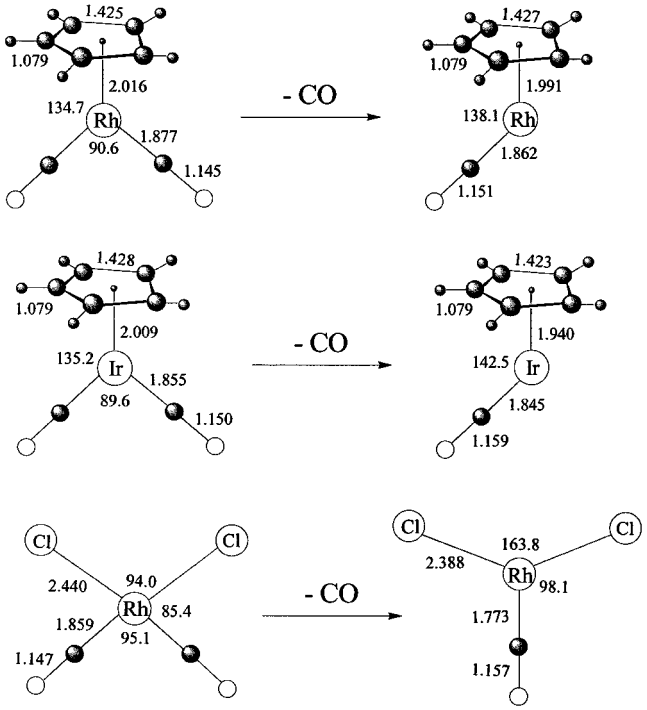

Figure 2. Optimized geometries of the dicarbonyl $CpRh(CO)_2$, $CpIr(CO)_2$, and $[Cl_2Rh(CO)_2]^-$ and the monocarbonyl CpRh(CO), CpIr(CO), and $[Cl_2Rh(CO)]^-$ in their singlet states using the B3LYP method. The large shaded circles denote carbon atoms, the blank circles denote the oxygen atoms, and the small shaded circles denote the hydrogen atoms, respectively.

shown in Figure 1 even though the orientation of the cyclopentadienyl of $CpM(CO)_2$ is different. Not only the geometries but also the energies of the two conformations of $CpM(CO)_2$ are essentially the same. The potential energy curves for the conversion of the two conformations are very flat (Table S3) indicating that there is no energy barrier between the two conformations. The potential energy surfaces of CO thermal dissociations should therefore be independent of the conformations of the parent molecules. The geometries of the molecules in the dissociation paths are also optimized and are collected in the Supporting Information (Table S2). The molecular shape and the geometrical parameters of CpM(CO) are very similar to their parent molecules. The $[Cl_2Rh(CO)]^-$ has a T-type structure compared to the square-planar structure of $[Cl_2Rh(CO)_2]^-$. The geometries of CpM(CO) are close to previous theoretical results.[11,14]

Figure 3 shows the potential energy curves of CO thermal dissociations in the present study with the zero of energy in each case taken to be the parent dicarbonyl molecules. Two significant features can be drawn from Figure 3. One is that the CO dissociation energies of $CpM(CO)_2$ are much higher than that of $[Cl_2Rh(CO)_2]^-$. The energy differences between the parent molecules and the resulting molecules are 73.4 kcal/mol for $CpIr(CO)_2$, 50.6 kcal/mol for $CpRh(CO)_2$, and 35.3 kcal/mol for $[Cl_2Rh(CO)_2]^-$. These results show that the generation of CpM(CO) and $[Cl_2Rh(CO)]^-$ is energetically unfavorable and that $CpIr(CO)_2$ needs the highest temperature to dissociate CO. Another feature is that the dissociation mechanisms of CO from $CpM(CO)_2$ and $[Cl_2Rh(CO)_2]^-$ are different. For $CpRh(CO)_2$ and $CpIr(CO)_2$, the potential energy curves are totally repulsive and the energy remains unchanged when the M−CO distance is larger than 4.0 Å. However, for $[Cl_2Rh(CO)_2]^-$, the Rh−CO

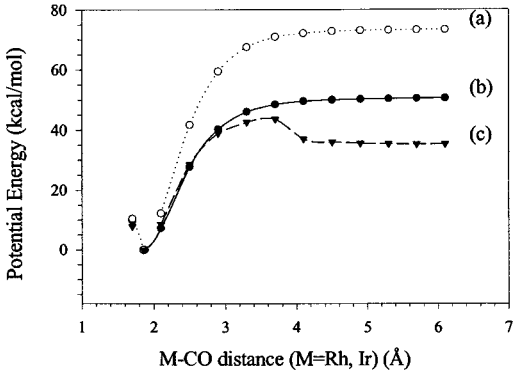

Figure 3. Potential energy curves of CO thermal dissociations from the parent dicarbonyl complexes calculated using the B3LYP method (a) $CpIr(CO)_2$, (b) $CpRh(CO)_2$, and (c) $[Cl_2Rh(CO)_2]^-$.

dissociation is an activation process with a transition state at a Rh−CO distance of about 3.7 Å. The transition state lies 41.4 kcal/mol higher than the parent $[Cl_2Rh(CO)_2]^-$ and 8.8 kcal/mol higher than the final product.[21] The energy needed to break the Rh−CO bond of $[Cl_2Rh(CO)_2]^-$ is therefore 41.4 kcal/mol instead of 35.3 kcal/mol. These results also imply that the reverse recombination mechanisms of CO to the monocarbonyl molecules are different. The recombination of CO to $[Cl_2Rh(CO)]^-$ is also an activation process, while the recombination of CO to CpM(CO) is a simple associative process. Our results are generally consistent with the experimental observation that the M−CO bond dissociation is difficult under thermal conditions. The expulsion of CO from $CpM(CO)_2$ and $[Cl_2Rh(CO)_2]^-$ can be achieved, however, by photoexcitation.

C. Excited States of $[Cl_2Rh(CO)_2]^-$. The calculated excitation energies, oscillator strengths, main configurations, and Mulliken population changes (relative to the ground state) are summarized in Table 1. The eight singlet excited states are composed of two A_1, three B_1, and three B_2 states. The molecular orbitals involved range from the 10 highest occupied orbitals to the 10 lowest virtual orbitals, the same case as those of $CpRh(CO)_2$ and $CpIr(CO)_2$, as discussed below. The diagrams of the most important orbitals involved are illustrated in Figure 4, and the important SCF orbitals are collected in the Supporting Information (Table S5). A common feature of the SCF orbitals shown in Figure 4 is that the occupied orbitals are the metal d orbitals and the metal−Cl antibonding or bonding orbitals and that the virtual orbitals have metal−CO antibonding or nonbonding characters. The nature of the excited state can be analyzed by means of the main configurations, orbital diagrams, and Mulliken population changes discussed below.

The excitation energies of the eight singlet excited states range from 3.57 to 5.37 eV. The three intense excited states are $1B_1$ at 3.57 eV, $2B_2$ at 4.61 eV, and $2A_1$ at 5.01 eV with oscillator strengths of 0.0726, 0.0652, and 0.0939, respectively. The oscillator strengths of the other excited states are weaker by more than an order of magnitude. The main configurations of the $1B_1$ state are ($16a_1$ $6b_1$) and ($16a_1$ $7b_1$). As shown in Figure 4, $16a_1$ is essentially an occupied d orbital of Rh, $6b_1$ is the lowest unoccupied molecular orbital (LUMO), and both $6b_1$ and $7b_1$ are the Rh−CO antibonding orbitals. Mulliken population changes show a clear metal to CO charge transfer in the $1B_1$ state: Rh has a charge loss of 0.334 and each CO has a charge increase of 0.201. Therefore, $1B_1$ is a typical MLCT excitation state and the electronic excitation to this state may lead to Rh−

Table 1. Excitation Energies, Oscillator Strengths, Main Configurations, and Mulliken Population Changes Calculated by the SAC/SAC−CI Method for $[Cl_2Rh(CO)_2]^-$

state	main configuration	excitation energy, eV	oscillator strength	population change[a] Δ(Rh)	Δ(CO)	Δ(Cl)
$1B_1$	$0.65(16a_1-6b_1)-0.60(16a_1-7b_1)$	3.57	0.0726	0.334	−0.201	0.033
$1B_2$	$-0.62(16a_1-16b_2)-0.53(16a_1-17b_2)-0.37(16a_1-15b_2)-0.26(15a_1-16b_2)$	3.58	0.0044	0.245	−0.082	−0.041
$2B_1$	$0.48(4a_2-16b_2)-0.46(3a_2-16b_2)-0.41(3a_2-17b_2)-0.37(4a_2-17b_2)$	4.26	0.0010	0.163	−0.092	0.010
$2B_2$	$0.52(4a_2-6b_1)+0.43(3a_2-6b_1)-0.41(4a_2-7b_1)-0.41(3a_2-7b_1)$	4.61	0.0652	0.150	−0.170	0.097
$1A_1$	$0.80(16a_1-19a_1)-0.33(16a_1-18a_1)+0.30(15a_1-18a_1)-0.20(16a_1-20a_1)$	4.70	0.0078	0.490	−0.284	0.038
$2A_1$	$0.48(4b_1-6b_1)+0.48(5b_1-6b_1)-0.44(4b_1-7b_1)-0.40(5b_1-6b_1)$	5.01	0.0939	0.230	−0.170	0.055
$3B_1$	$0.65(17a_1-6b_1)-0.48(17a_1-7b_1)-0.35(14a_1-7b_1)+0.34(14a_1-6b_1)$	5.17	0.0041	−0.001	−0.194	0.194
$3B_2$	$0.67(16a_1-17b_2)-0.57(16a_1-16b_2)+0.28(15a_1-17b_2)-0.20(15a_1-16b_2)$	5.37	0.0002	0.569	−0.321	0.035

[a] Mulliken population change corresponds to the charge difference between the excited state and the ground state.

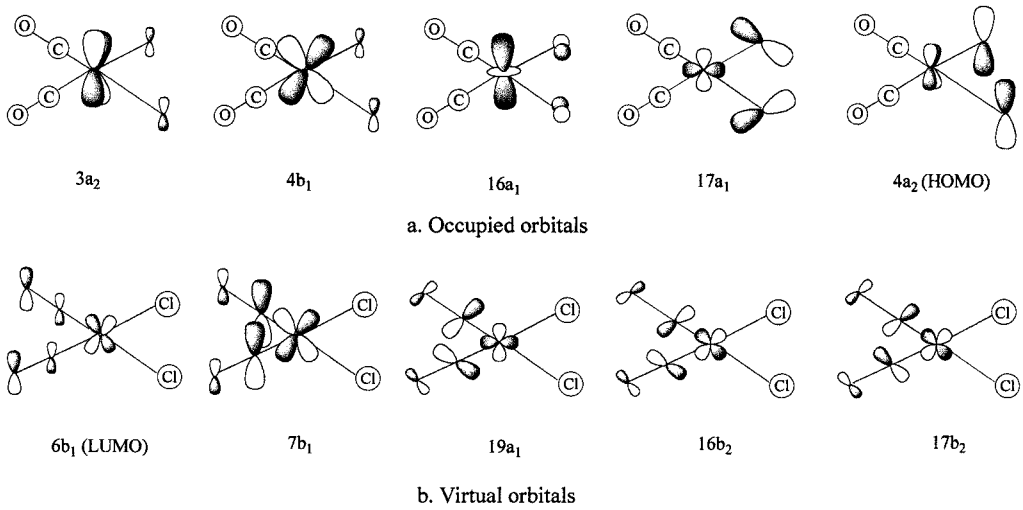

Figure 4. Diagrams of the most important SCF orbitals involved in the excited states of $[Cl_2Rh(CO)_2]^-$, (a) occupied orbitals and (b) virtual orbitals.

Table 2. Excitation Energies, Oscillator Strengths, Main Configurations, and Mulliken Population Changes Calculated by the SAC/SAC−CI Method for $CpRh(CO)_2$

state	main configuration	excitation energy, eV	oscillator strength	populatio n change[a] Δ(Rh)	Δ(CO)	Δ(Cp)
1A"	−0.72(24a'−18a")−0.51(24a'−17a") −0.26(22a'−18a")−0.25(24a'−20a")	2.71	0.0000	−0.109	−0.038	0.184
2A"	0.78(23a'−18a")−0.49(23a'−17a") +0.31(23a'−20a")	3.22	0.0081	0.224	−0.072	−0.080
1A'	0.69(15a"−18a")+0.43(15a"−17a") +0.25(15a"−20a")+0.23(24a'−28a')	3.95	0.0000	0.231	−0.117	0.004
2A'	0.42(23a'−27a')−0.41(23a'−25a') −0.37(24a'−28a')+0.31(24a'−27a')	4.38	0.0116	0.246	−0.218	0.190
3A'	0.46(23a'−27a')−0.46(23a'−25a') +0.34(24a'−28a')−0.29(23a'−28a')	4.45	0.0359	0.246	−0.201	0.157
4A'	0.73(24a'−25a')−0.44(24a'−27a') −0.26(24a'−28a')	4.57	0.1671	−0.146	−0.122	0.391
3A"	−0.74(21a'−18a")−0.46(21a'−17a") −0.38(21a'−20a")	4.84	0.0045	0.169	−0.048	−0.073
4A"	−0.47(24a'−18a")+0.47(22a'−18a") +0.43(22a'−17a")+0.39(24a'−17a")	5.86	0.0012	−0.318	−0.034	0.387

[a] Mulliken population change corresponds to the charge difference between the excited state and the ground state.

CO bond breaking. The main configurations of $2B_2$ are ($4a_2$ $6b_1$), ($3a_2$ $6b_1$), ($4a_2$ $7b_1$), and ($3a_2$ $7b_1$). $4a_2$ is the highest occupied molecular orbital (HOMO) and is dominated by the p character of Cl with Rh−Cl antibonding character and $3a_2$ is a d orbital of Rh. This is also a MLCT excitation state as shown by the population changes. The main configurations of $2A_1$ are ($4b_1$ $6b_1$), ($5b_1$ $6b_1$), ($4b_1$ $7b_1$), and ($5b_1$ $7b_1$). Both $4b_1$ and $5b_1$ are d orbitals of Rh, and Mulliken population changes again show a clear metal to CO charge-transfer excitation. The main orbitals involved in other excited states are the occupied $3a_2$, $4a_2$, $16a_1$, and $17a_1$ orbitals and the virtual $16b_2$, $17b_2$, $18a_1$, $19a_1$, and $20a_1$ orbitals. $17a_1$ is the p orbital of Cl with a weak Rh−Cl antibonding interaction. $16b_2$ and $17b_2$ are the Rh−CO nonbonding orbitals and $18a_1$ and $20a_1$ are the Rydberg orbitals of Rh, C, and O. Electronic excitation into these orbitals may lead to intramolecular charge rearrangement which has less effect for the metal−CO bond breaking. These excited states are therefore less important for the reactions involving metal ion oxidation and they are actually much weaker than the MLCT states.

D. Excited States of $CpRh(CO)_2$ and $CpIr(CO)_2$. For $CpRh(CO)_2$ and $CpIr(CO)_2$, we calculated four A' and four A" singlet excited states. The calculated excitation energies, oscillator strengths, main configurations, and Mulliken population changes for $CpRh(CO)_2$ are summarized in Table 2 and the diagrams of the most important orbitals involved are illustrated in Figure 5. As shown in Figure 5, the occupied orbitals are metal d orbitals and metal−Cp antibonding or bonding orbitals, and the virtual orbitals are the metal−CO antibonding or nonbonding orbitals.

The lowest excited singlet state is calculated to be 1A" at 2.71 eV with zero oscillator strength. The main configurations

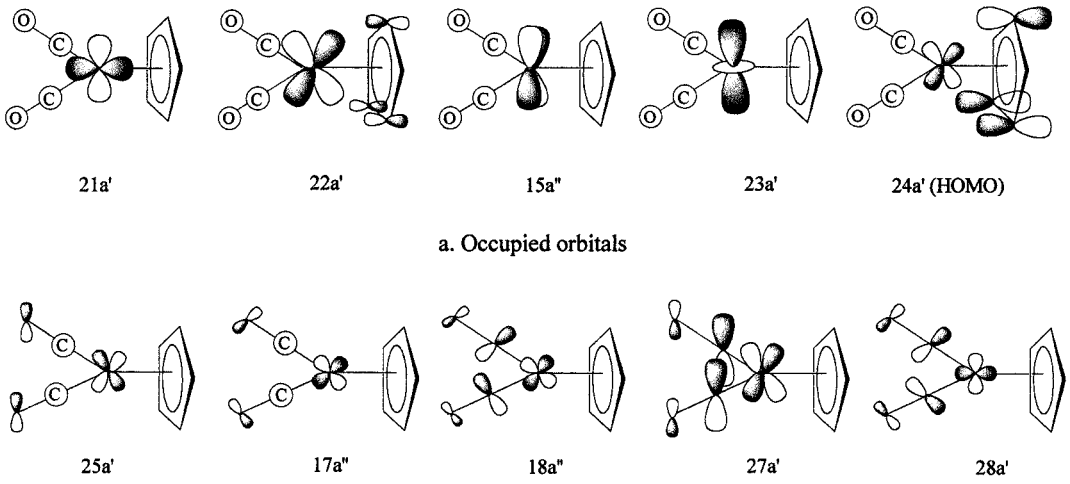

Figure 5. Diagrams of the most important SCF orbitals involved in the excited states of $CpRh(CO)_2$ and $CpIr(CO)_2$, (a) occupied orbitals and (b) virtual orbitals. 25a' is the LUMO of $CpRh(CO)_2$ and 17a" is the LUMO of $CpIr(CO)_2$. The 27a' and 28a' orbitals of $CpRh(CO)_2$ shown in this figure are exchanged to be 28a' and 27a' for the case of $CpIr(CO)_2$.

Table 3. Excitation Energies, Oscillator Strengths, Main Configurations, and Mulliken Population Changes Calculated by the SAC/SAC−CI Method for $CpIr(CO)_2$

				populatio n change[a]		
state	main configuration	excitation energy, eV	oscillator strength	Δ(Rh)	Δ(CO)	Δ(Cp)
1A"	0.66(24a'−17a")−0.66(24a'−18a")	3.30	0.0000	−0.067	−0.068	0.183
2A"	0.69(23a'−18a")−0.65(23a'−17a")	3.84	0.0073	0.235	−0.110	−0.035
1A'	0.53(24a'−29a')+0.43(15a"−18a") −0.37(15a"−17a")+0.36(24a'−26a')	4.55	0.0002	0.216	−0.194	0.153
2A'	0.67(23a'−28a')−0.62(23a'−25a')	4.93	0.0335	0.242	−0.171	0.080
3A'	0.79(24a'−25a')−0.48(24a'−28a')	5.00	0.2132	−0.253	−0.052	0.338
4A'	0.53(15a"−18a")−0.51(15a"−17a") −0.33(24a'−29a')−0.33(24a'−26a')	5.13	0.0140	0.139	−0.121	0.072
3A"	−0.80(24a'−20a")+0.31(24a'−21a")	5.15	0.0001	0.264	−0.229	0.195
4A"	−0.58(23a'−20a")−0.50(24a'−19a") −0.27(22a'−20a")−0.26(23a'−17a")	6.20	0.0188	0.329	−0.170	0.009

[a] Mulliken population change corresponds to the charge difference between the excited state and the ground state.

of 1A" are (24a' 18a"), (24a' 17a"), (22a' 18a"), and (24a' 20a"). 24a' is the HOMO with metal−Cp antibonding character dominated by the p character of Cp and 22a' is the metal−Cp bonding occupied orbital dominated by metal d character. 17a", 18a", and 20a" are the metal−CO nonbonding virtual orbitals with metal, C, and O Rydberg orbital characters. As a result, electronic excitation to this state has no effect for the metal−CO bond photoactivation. Mulliken population changes show that the charge transfer is from the ligand Cp to the metal and CO. The intramolecular charge rearrangement may result in a structural change. This excited state compares to the photochemical experiment of $CpRh(CO)_2$ in the long-wavelength irradiation at 458 nm (2.71 eV).[7b,c]

The important excitations are the A' excited states in the range of 4.3 ∼ 4.6 eV. Interestingly, the strongest excitation is found to be 4A' at 4.57 eV with the main configurations of (24a' 25a'), (24a' 27a'), and (24a' 28a'). 25a' is the LUMO with metal, C, and O Rydberg orbital characters and 27a' and 28a' are metal−CO antibonding orbitals. 24a' is the HOMO dominated by the p orbitals of Cp as discussed above. Although the electrons can be excited into the metal−CO antibonding orbitals, the predominant excitation is from 24a' to 25a', namely, from the p orbitals of Cp to the Rydberg orbitals of Rh, C, and O. Mulliken population changes also confirm that the charge transfer is not from the metal to CO but from the ligand Cp to the metal and CO. So, this excited state is not the MLCT excitation. The MLCT excitations are found to be 2A' at 4.38 eV and 3A' at 4.45 eV with considerable oscillator strengths. The predominant configurations are (23a' 27a') and (23a' 25a') for both 2A' and 3A' states. As shown in Figure 5, 23a' is a typical d orbital of the metal, and the electronic excitations at these states result in the charge transfer from the metal d orbital to Rh−CO antibonding orbitals. Other excited states are much weaker than the excited states discussed here and correspond to electronic excitation into the 17a" and 18a" Rh−CO nonbonding orbitals.

The calculated excitation energies, oscillator strengths, main configurations, and Mulliken population changes for $CpIr(CO)_2$ are summarized in Table 3. The excited states of $CpIr(CO)_2$ are essentially similar to those of $CpRh(CO)_2$ except for the higher excitation energies and minor configuration differences. The orbital diagrams shown in Figure 5 are generally common for both $CpIr(CO)_2$ and $CpRh(CO)_2$ with the exceptions that 17a" turns out to be the LUMO for $CpIr(CO)_2$ and the 27a' and 28a' orbitals of $CpRh(CO)_2$ shown in Figure 5 are reversed for the case of $CpIr(CO)_2$. The lowest excited state is again 1A" but at 3.30 eV with the main configurations of (24a' 17a") and (24a' 18a"). This excited state corresponds to the charge transfer from the ligand Cp to the metal−CO nonbonding orbitals with Rydberg character, and it compares to the photochemical experimental value for $CpIr(CO)_2$ at 366 nm (3.40 eV).[7a]

The most interesting excitations correlating to the photoreactions of $CpIr(CO)_2$ are the A' excited states at about 5.0 eV. The strongest excitation is the 3A' at 5.00 eV for $CpIr(CO)_2$ compared with the 4A' at 4.57 eV for $CpRh(CO)_2$. This

Table 4. Comparison of the Calculated Metal (Rh 4d, Ir 5d) to CO π^* Charge-Transfer Excitation Energies with Experimental Spectra for $[Cl_2Rh(CO)_2]^-$, $CpRh(CO)_2$, and $CpIr(CO)_2$

	state	excitation energy, eV	expt, eV
$[Cl_2Rh(CO)_2]^-$	$1B_1$	3.57	3.7[a]
	$2B_2$	4.61	4.6[a]
	$2A_1$	5.01	
$CpRh(CO)_2$	2A'	4.38	4.34[b]
	3A'	4.45	
$CpIr(CO)_2$	2A'	4.93	

[a] Experimental absorption spectra of $[(n\text{-}C_4H_9)_4N][Cl_2Rh(CO)_2]$ from ref 31d. [b] Ref 7d.

is the ligand Cp to metal and CO charge-transfer excited state as discussed for the 4A' excited state of $CpRh(CO)_2$. The MLCT excitation is found to be the 2A' state at 4.93 eV with the main configurations of (23a' 28a') and (23a' 25a'). Both 23a' and 25a' are metal d orbitals as $CpRh(CO)_2$ and 28a' is the Ir−CO antibonding orbital corresponding to the 27a' orbital diagram of $CpRh(CO)_2$ shown in Figure 5. The 4A' state at 5.13 eV has the main configurations of (15a'' 18a'') and (15a'' 17a''). 15a'' is the d orbital of Ir, and 18a'' and 17a'' are the Ir−CO nonbonding virtual orbitals with the Ir, C, and O Rydberg orbital characters. This excitation does not contribute to the Ir−CO bond photoactivation although it is a metal to CO charge-transfer excitation. Despite the similar features of the main excited states, the SCF orbitals involved in other excited states of $CpIr(CO)_2$ have wider diversity than those of $CpRh(CO)_2$.

E. Discussion and Comparison with the Experiment. Table 4 summarizes the calculated metal (Rh 4d, Ir 5d) to CO π^* charge-transfer excitation energies for $[Cl_2Rh(CO)_2]^-$, $CpRh(CO)_2$, and $CpIr(CO)_2$. The available experimental spectra are included for comparison. MLCT excitations have been characterized in great detail for the square-planar complexes with d^8 electronic configurations.[31] Geoffroy et al.[31d] have reported the electronic absorption spectra of some square-planar Rh(I) and Ir(I) complexes. Our computed values for $1B_1$ at 3.57 eV and $2B_2$ at 4.61 eV correlate very well with the two absorption bands observed at 3.7 and 4.6 eV for $[(n\text{-}C_4H_9)_4N][Cl_2Rh(CO)_2]$.[31d] The present results for $[Cl_2Rh(CO)_2]^-$ are also in line with the experimental values of 3.9 and 4.8 eV for the chloro-bridged dimer $[ClRh(CO)_2]_2$[31e] and 3.9 and 4.6 eV for $Rh(CO)_2/Al_2O_3$[32] surface species. The close similarity between the theoretical and experimental results indicates that $[Cl_2Rh(CO)_2]^-$ is a good model molecule for the study of the electronic structures and excitations of these kinds of molecules. Experimentally, Yates et al.[33] have reported that the $Rh(CO)_2/Al_2O_3$ surface species is also effective for C−H bond activation in methane and cyclohexane and for H−H bond activation in H_2 under UV irradiation. Since all the intense excitations are identified to be the MLCT excitations which lead to the expulsion of CO for the case of $[Cl_2Rh(CO)_2]^-$ in the present study, it is reasonable to deduce that the surface reactions proceed via the photoproduced $Rh(CO)/Al_2O_3$ surface intermediate.

In contrast to those of $[Cl_2Rh(CO)_2]^-$, the MLCT excitations of $CpRh(CO)_2$ and $CpIr(CO)_2$ exist only in the higher energy states. The MLCT excitations of $CpRh(CO)_2$ are calculated to be 2A' at 4.38 eV and 3A' at 4.45 eV. These states correspond to the experimental absorption band of $CpRh(CO)_2$ at 286 nm (4.34 eV).[7d] For $CpIr(CO)_2$, the MLCT excitation is calculated to be 2A' at 4.93 eV. These results imply that the photochemistry of $CpM(CO)_2$ is different from that of $[Cl_2Rh(CO)_2]^-$.

An important observation in the present study is the identification of two different types of excited states involved in the photochemistry of $CpRh(CO)_2$ and $CpIr(CO)_2$. One is the ligand Cp to metal and CO charge transfer excitation which appear in both long-wavelength and short-wavelength irradiations with different characteristics. Another is the MLCT excitations which exist only in the short-wavelength irradiation. These results provide valuable theoretical insight into the photochemical experiments performed by Lees et al.[7,8] On the basis of their wave-dependent quantum efficiency measurement, Lees et al.[7c,d,8b] proposed a photophysical representation of the low-energy excited states and their reactivities in $CpRh(CO)_2$, $Cp^*Rh(CO)_2$, and $(HBPz_3^*)Rh(CO)_2$. Two different types of excited states are suggested in the photophysical representation and a ($\eta^5-\eta^3$) ring slippage mechanism is proposed for the ligand photosubstitution at the lower energy state. The photoinitiated $(\eta^3\text{-}Cp)Rh(CO)_2$ may undergo rapid intersystem crossing to corresponding triplet ligand field excited states or undergo rapid reversible ring slippage to relax back to the ground state. The wavelength dependence of the quantum efficiencies for the C−H/Si−H bond activations and ligand photosubstitution of $CpM(CO)_2$[7,8] can be understood by the existence of the two different types of excited states discussed above. A M−Cp* bond breaking mechanism suggested from the photolysis study of $Cp^*Rh(CO)_2$[34] is unlikely to occur as the M−Cp antibonding orbital is an occupied orbital instead of a virtual orbital involved in the excited states. In contrast, charge transfer from the M−Cp antibonding orbital to the Rh−CO antibonding or nonbonding virtual orbitals may strengthen the M−Cp bond interaction.

A competitive charge-transfer mechanism in the photochemistry of $CpRh(CO)_2$ and $CpIr(CO)_2$ identified in the present study enables us to provide a theoretical explanation for the low quantum efficiencies for the C−H bond activation of $CpRh(CO)_2$ and $CpIr(CO)_2$. The quantum efficiency depends on the proportion of the CpM(CO) intermediate produced in the higher energy excited states. Since the metal to CO charge transfer excitation and the ligand Cp to metal and CO charge transfer excitation are mixed in the higher excited states and the ligand Cp to metal and CO charge transfer excitation is much stronger than the MLCT excitation, the proportion of the CO photodissociation is relatively small. The origin of the low quantum efficiencies for the C−H bond activation is therefore not only attributed to the existence of lower lying excited states below the stronger MLCT band explained by Bromberg et al.[9] but mainly attributed to the smaller proportion of the MLCT excitation in the higher energy excited states.

(31) (a) Geoffroy, G. L.; Wrighton, M. S.; Hammond, G. S.; Gray, H. B. *J. Am. Chem. Soc.* **1974**, *96*, 3105. (b) Isci, H.; Mason, W. R. *Inorg. Chem.* **1975**, *14*, 913. (c) Brady, R.; Plynn, B. R.; Geoffroy, G. L.; Gray, H. B.; Peone, J., Jr.; Vaska, L. *Inorg. Chem.* **1976**, *15*, 1485. (d) Geoffroy, G. L.; Isci, H.; Litrenti, J.; Mason, W. R. *Inorg. Chem.* **1977**, *16*, 1590. (e) Epstein, R. A.; Geoffroy, G. L.; Keeney, M. E.; Mason, W. R. *Inorg. Chem.* **1979**, *18*, 478.
(32) Wovchko, E. A.; Zubkov, T. S.; Yates, J. T., Jr. *J. Phys. Chem.* **1998**, *102*, 10535.
(33) (a) Ballinger, T. H.; Yates, J. T., Jr. *J. Phys. Chem.* **1992**, *96*, 9979. (b) Wong, J. C. S.; Yates, J. T., Jr. *J. Am. Chem. Soc.* **1994**, *116*, 1610. (c) Wovchko, E. A.; Yates, J. T., Jr. *J. Am. Chem. Soc.* **1995**, *117*, 12557. (d) Wong, J. C. S.; Yates, J. T., Jr. *J. Phys. Chem.* **1995**, *99*, 12640.
(34) Pradella, F.; Rehorek, D.; Scoponi, M.; Sostero, S.; Traverso, O. *J. Organomet. Chem.* **1993**, *453*, 283.
(35) Pollak, C.; Rosa, A.; Baerends, E. J. *J. Am Chem. Soc.* **1997**, *119*, 7324.
(36) Rosa, A.; Baerends, E. J.; Gisbergen, S. J. A.; Lenthe, E.; Groeneveld, J. A.; Snijders, J. G. *J. Am Chem. Soc.* **1999**, *121*, 10356.
(37) Guillaumont, D.; Daniel, C. *J. Am. Chem. Soc.* **1999**, *121*, 11733.

Since our interest centers mostly on the nature of the excited states of the title compounds, the metal−CO photodissociation mechanism has not been considered in this paper. Both the geometry distortion and the crossing with the potential energy curves of the states during ligand expulsion are important for understanding the photodissociation mechanisms of transition-metal carbonyl complexes.[35−37]

VI. Conclusions

We have investigated the molecular structures and the excited states of $CpM(CO)_2$ and $[Cl_2Rh(CO)_2]^-$ complexes using the B3LYP and the SAC/SAC−CI theoretical methods. All the dicarbonyl complexes have singlet ground electronic states with large singlet−triplet separations. Large geometry differences between the singlet and triplet states have been found with a linear M−C−O bond in the singlet states and a bent M−C−O bond in the triplet states. Thermal dissociations of CO from the parent dicarbonyls are energetically unfavorable and $CpIr(CO)_2$ needs the highest energy to dissociate CO. CO thermal dissociation is an activation process for $[Cl_2Rh(CO)_2]^-$ while it is a repulsive potential for $CpM(CO)_2$.

The different excitation features of $CpM(CO)_2$ and $[Cl_2Rh(CO)_2]^-$ have been identified in the present excited-state study. For $[Cl_2Rh(CO)_2]^-$, all the intense excitations are identified to be the MLCT excitations resulting in the photodissociation of CO from $[Cl_2Rh(CO)_2]^-$. A significant feature of the excited states of $CpM(CO)_2$ is that the strongest excitation corresponds to the ligand Cp to metal and CO charge transfer which lies in the same energy range as the MLCT excitation bands. The lowest excited state corresponds to electronic excitation from a metal−Cp antibonding orbital to a metal−CO nonbonding orbital. Electronic excitation to this state may have little effect for the M−CO bond photoactivation. The photodissociation of CO from $CpM(CO)_2$ can be achieved in the higher energy levels; however, since a ligand Cp to metal and CO charge-transfer excitation is stronger than the MLCT excitation, the proportion of CO photodissociation should be small. A competitive charge-transfer mechanism in the photochemistry of $CpM(CO)_2$ is responsible for the low quantum efficiencies for the C−H bond activation. The wavelength dependence of the quantum efficiencies for the C−H/Si−H bond activations and ligand photosubstitution of $CpM(CO)_2$ can be explained by the existence of the two different types of excited states of $CpM(CO)_2$.

Acknowledgment. This work was supported by grants from the Natural Sciences and Engineering Research Council of Canada (NSERC) and the Killam Trusts (R.J.B.) and by a Grant-in-Aid for Scientific Research from the Ministry of Education, Science, Culture, and Sports of Japan (H.N.).

Supporting Information Available: Archive entries of the B3LYP optimized geometries and energies (Table S1), summary of optimized potential surface scans by B3LYP (Table S2), potential energies between the two conformations of $CpRh(CO)_2$ and $CpIr(CO)_2$ (Table S3), SAC/SAC−CI calculation results (Table S4), and some important SCF occupied and unoccupied molecular orbitals (Table S5) (PDF). This material is available free of charge via the Internet at http://pubs.acs.org.

JA0108178